TNO-report
98-MIT-NM-R /1623

Compaction and subsidence study of the Ameland gas-field with creep effects

TNO Building and Construction Research

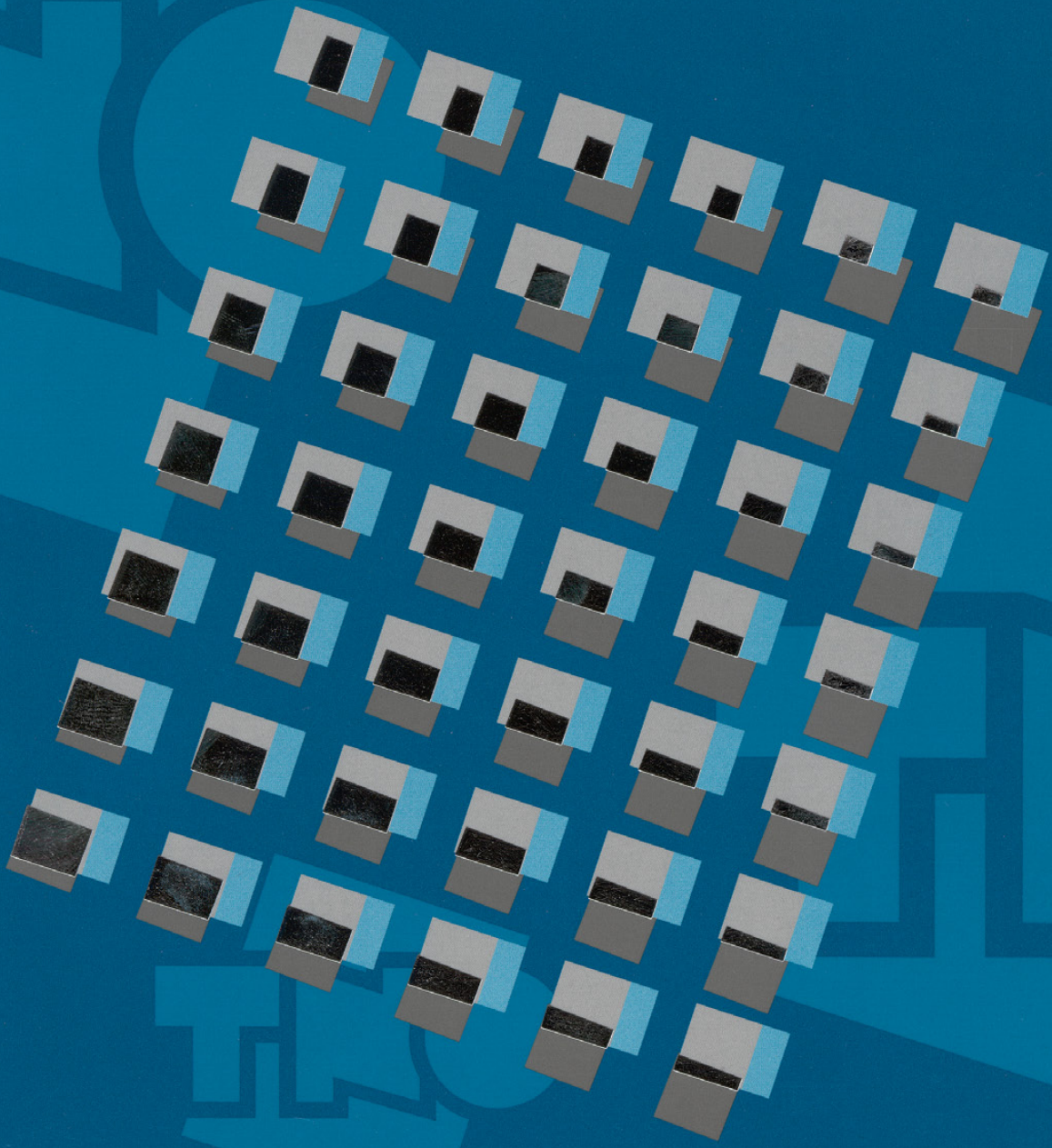

TNO-report
98-MIT-NM-R /1623

Compaction and subsidence study of the Ameland gas-field with creep effects

TNO Building and Construction Research

Date
December 1998

Author(s)
dr.ir. G. Schreppers

Contact person
dr.ir. G. Schreppers

Lange Kleiweg 5
P.O. Box 49
2600 AA Delft
The Netherlands

Phone +31 15 284 20 00
Fax +31 15 284 39 90

Sponsor : Nederlandsche Aardolie Maatschappij BV, Assen

Monitoring Agency : Shell Exploration and Production BV, Research and Technical Services, Rijswijk

All rights reserved.
No part of this publication may be reproduced and/or published by print, photoprint, microfilm or any other means without the previous written consent of TNO.

In case this report was drafted on instructions, the rights and obligations of contracting parties are subject to either the Standard Conditions for Research Instructions given to TNO, or the relevant agreement concluded between the contracting parties. Submitting the report for inspection to parties who have a direct interest is permitted.

Projectnumber : 8.23.6.4238
Approved : dr.ir. M. Hendriks

Number of pages : 37

© 1998 TNO

TNO Building and Construction Research provides a comprehensive research and development service specifically geared to the needs of the construction and engineering industry.

Netherlands Organization for Applied Scientific Research (TNO)

Summary

Title	:	Compaction and subsidence study of the Ameland gas-field with creep effects
Authors	:	dr.ir. G. Schreppers
Datum	:	December 1998
Opdrachtnr.	:	8.23.6.4238
Rapportnr.	:	98-MIT-NM-R /1623

The Ameland reservoir is a gas-field at circa 3300 meters depth, situated in the Upper Slochteren sandstone formation, which is circa 90 meters thick. The reservoir has a diameter of 15-20 km.

A 3-dimensional finite element model has been developed in this study for the reservoir, the overburden layers and the layers below the reservoir. For 5-years time-intervals in the period 1986-2020, the depletion pressure-distribution in the reservoir has been derived from a reservoir analysis study by NAM. The maximum depletion pressure is 52 MPa. The stiffness properties of the different formations are partly derived from seismic velocities (most non-reservoir layers) and partly from experiments on samples (reservoir and salt layers). For the Upper Slochteren reservoir the stiffness is related to the measured porosity distribution, and the porosity-stiffness relation is calibrated against laboratory experiments and against values from an inversion study with SUBSINV. The Zechstein salt-layer in the overburden has a very strong varying thickness. Special attention is paid in this study to creep-effects in the Zechstein salt. For this purpose the creep model of Fokker [6] is applied which leads to reduction of shear stresses as function of time.

In this study, parameter variations with respect to the stiffness of the reservoir formation, the creep properties of the Zechstein salt formation and with respect to the pressure distribution in the reservoir are carried out using the program DIANA. The results are presented and discussed, and compared with results achieved with the program SUBCAL and with surface subsidence measurements.

From this study it is concluded that a realistic estimate for the maximum surface subsidence is 26.5 cm at the end of field life, and a worst case maximum is 32 cm. The estimated volume of the surface subsidence bowl is 14 million cubic meters at the end of field-life.

Contents

1. Introduction

1.1 Characterization of the study

The Ameland gas-field is situated at a depth of circa 3.3 km in the Southern part of the North Sea, partially under the island Ameland in the Netherlands. The diameter of the reservoir is 15-20 km with the Upper Slochteren unit (ROSLU) being depleted. The compacting thickness of this layer is circa 90 m.

A 3-dimensional linear elastic numerical model is used to predict the reservoir compaction and the surface subsidence.

In this study special attention is paid to the supposed salt-creep in the overburden, which was suspected to be the major reason that the actual measured subsidence is taking place at a higher rate (cm/year) than the predicted subsidence with more simple models.
The numerical model used for the analysis, is the program GEOMEC, which is a compaction special under development, derived from the program DIANA.

1.2 Objectives of the study

To identify

- surface subsidence as function of depletion pressure and time,
- volume of subsidence bowl as function of depletion pressure and time,
- reservoir compaction as function of depletion pressure and time, and
- lateral stress support in reservoir as function of depletion pressure and time.

Further, the creep effects in the salt-layers in the overburden are identified.

1.3 Structure and scope of the study

In chapter 2 the 3-dimensional finite element model and the different formation layers with their respective material properties are defined. For all the different formations in the model a linear elastic behavior is assumed. However, for the Zechstein salt-layer a parameter study is made taking nonlinear shear-stress relaxation into account. The depletion pressures and reservoir size (depleting area) for different times, which are the driving force in the reservoir compaction and surface subsidence, are derived form reservoir analyses. For this purpose the depletion pressure may vary in the horizontal plane, but is assumed to be constant over the

thickness of the reservoir. Only the Upper Slochteren formation is depleted. Faults are not considered in this study.

In chapter 3 the results are described and discussed. First, a reference model with a constant value of the reservoir stiffness is considered. Second, a model with the reservoir stiffness being related to the measured reservoir porosity is taken into account. The creep-effects of the salt-layer in the overburden are studied by assuming Halite, Carnalite and Bischofite characteristics. For all models being analyzed the surface subsidence, reservoir compaction strain and the reduction of horizontal stresses in the reservoir are visualized for 5-year time steps in the period 1990-2020. As the depletion pressure distribution is one of the main factors affecting the subsidence results for this model, a worst case scenario is defined, where the depletion pressure is assumed to be constant at the maximum value for all points in the reservoir.

Conclusions are given in chapter 4.

2. Model definition

2.1 3-dimensional model

The Ameland gasfield is located in the Southern part of the North Sea, just under the island Ameland in the Netherlands. Figure 1 shows a schematized plot of the localization of the gas-field (red-contour) and the island (yellow). The X-axis in this figure is pointing to the East, while the Y-axis is pointing to the North. The green-lines in Figure 1 show the top-view of the 3-dimensional finite element grid for the Ameland gas-field. In the center finer elements (500 x 500 m) have been chosen in order to achieve more accurate results, while at the outer edges the grid is courser (2000 x 2000 m) in order to save computer calculation time.

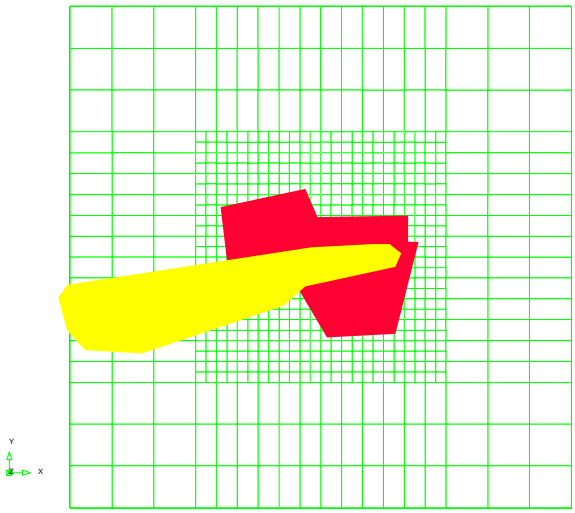

Figure 1 Schematized localization of Ameland gas-field

The total dimensions of the element model in the horizontal plane are 24 x 24 km.

The following approach has been chosen to make a 3-dimensional model.

NAM provided for every grid-point in Figure 1 the depths of the top-surfaces of the following rock-layers:

- North Sea
- Chalk
- Cretacious
- Jurrassic
- Zechstein
- Anhydrite
- Ten Boer (ROCLT)
- Upper Slochteren (ROSLU)

- Ameland claystone (ROCLA)
- Lower Slochteren
- Limburg

The top of the model is chosen at seabed level, at 0 meter depth, and the bottom at 5000 m depth, which is in the Limburg layer. From top chalk to seabed, a homogeneous layer of sediments is assumed.

Some very small modifications have been applied to the geometry data of the top-layers provided by NAM at those points where the top-layers intersected each other. At those points a minimum thickness of 1 meter is assumed, and the respective top-layer depths are adapted. The Zechstein salt-layer is modeled differently. At the top of Zechstein the formation is found to be softer than in lower regions in the Zechstein. This soft layer is identified as a squeezing salt-layer. In fact the squeezing salt is a broken layer with strong variations in the material properties. In this model the Zechstein formation is described by 3 sub-layers (see Table 1): A top-layer with a constant thickness of 20 m (noticed as Zechstein20), a layer with a constant thickness of 80 m (noticed as Zechstein80) and the remaining thickness of Zechstein (noticed as Zechstein). Now a block is defined with 12 changing surfaces, which do not intersect and are all covering the full horizontal domain of the block.

For every layer in the vertical direction a number of elements is assumed that is constant over the full horizontal domain. The sediments, or Northsea layer is divided in 1 element-layer, the chalk, Cretacious and Jurrassic layers are divided in 2 element-layers each, the Zechstein20 and Zechstein 80 layers have only 1 element-layer each and the Zechstein 2. All the other formation-layers are constituted by 1 element-layer each, except the Limburg layer which has 4 element-layers.

With these assumptions a finite element model has been created. The model is composed of HX24L elements which is a brick element with 8 nodes and linear interpolation of displacements in the X-, Y- and Z-direction.

In the nodes at the bottom of the model the displacements in vertical direction are supported, while at the boundaries at front, back, left and right side the displacements in the normal direction are supported. At the top-surface all nodes are free to move.

In Figure 2 the 3-dimensional model is shown from a South/East view-point. In this figure all formation layers are displayed with different colors (see Table 1 for color-identification) and the changing depth and thickness of the layers can be easily recognized in this figure. The black frame at the top of the model is the transition between the finer and the coarser grid. This frame can be used as marker for the reservoir area. Figure 3 is equal to Figure 2, but now the finite element grid is drawn too. The figure shows a strong variation of the thickness of the elements in the model.

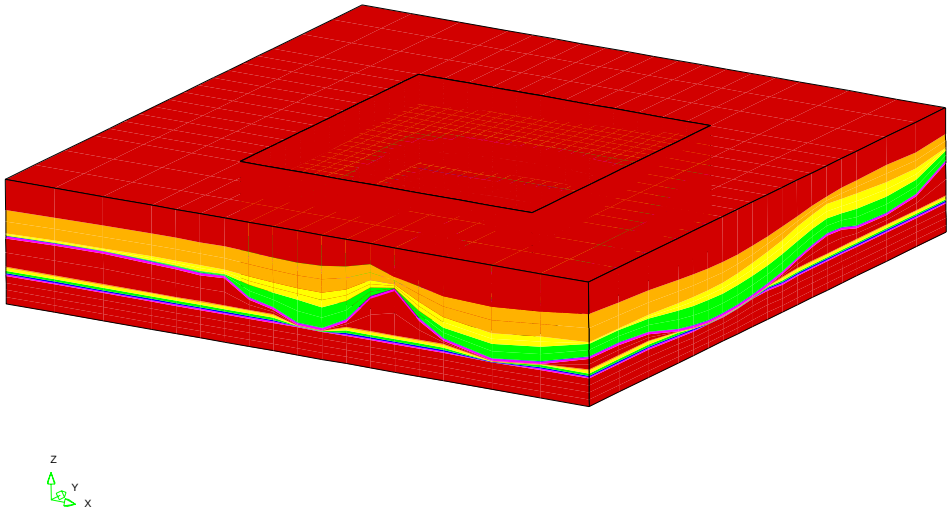

Figure 2 Rock-layer identification

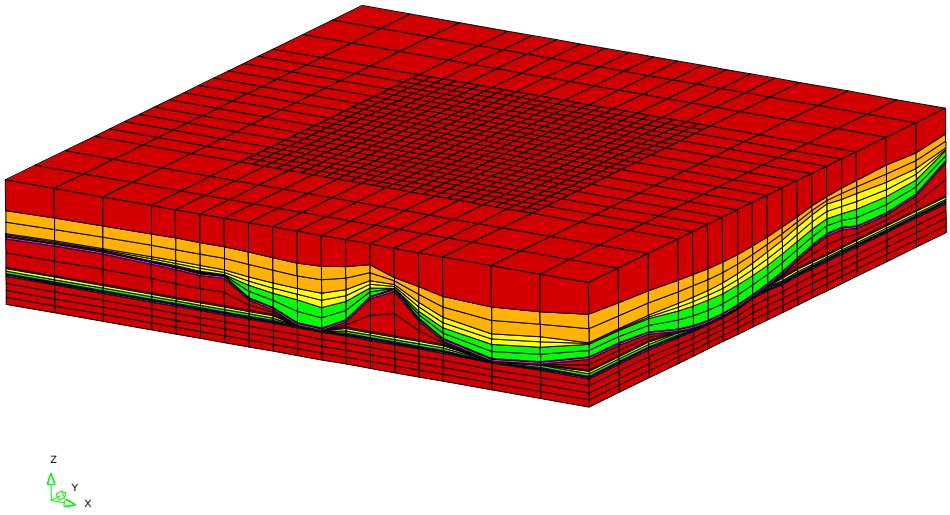

Figure 3 Finite Element Model

In Figure 4 a West-East cross-section through the model is shown with a zoom-in to the reservoir area in the cross-section. At the left- and right-end of the figure the transition-lines from the coarser to the finer grids can be recognized. From this figure it can be noticed that the Zechstein salt-layer is very thick just over the reservoir, while it is thin at the outer edges. At the location where the Zechstein layer is thick, the 3 overlying layers (Chalk, Cretacious and Jurrassic) are thinner. Figure 5 show another cross-section through the model and from this figure it can be concluded that the thick ridge of Zechstein salt-layer expands in Northern direction,

while in the South/Western corner of the reservoir the thickness of the Zechstein is minimal.

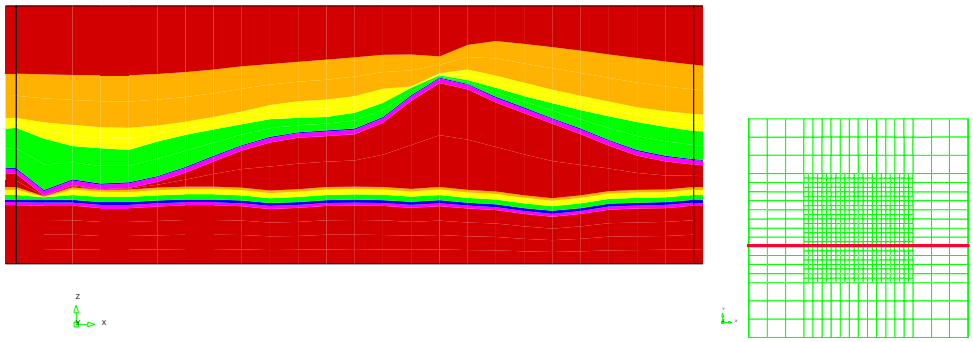

Figure 4 West/East cross-section

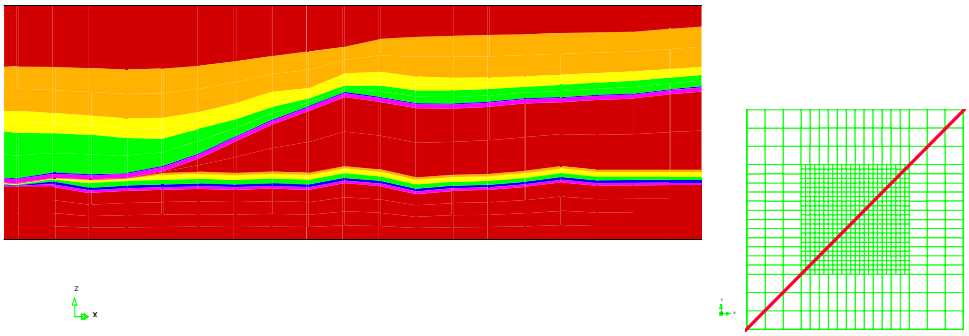

Figure 5 West/South - East/North cross-section

2.2 Material characterization

2.2.1 Overburden and layers below the producing reservoir

The rock material parameters for the various layers are obtained from different sources (see Table 1). For most layers present in the overburden and below the producing reservoir, Young's moduli and Poisson's ratios are derived from average (no depth trend applied) primary (*Vp*) and secondary (*Vs*) sonic wave velocities and average densities (Ref. 1). *Vp* values are readily available from seismic surveys, *Vs* values however are less easy to obtain. Therefore, a generally by NAM used relationship between *Vp* and *Vs* is used (Ref. 2). Since the Young's moduli derived from sonic wave velocities are dynamic values (*Ed*), a conversion to static values (*Es*) takes place using

$$Es = 0.5 * Ed$$

for sandstone and

$$Es = 0.41 * Ed - 1.4$$

for shales (Ref. 3). These values are compared with values in previous studies and slightly adjusted, as required (Ref. 4, 5).

Lithologies	Color	Source	Young modulus [GPa]	Poisson ratio [-]
Northsea	red	Ref. 1 & 2	2.0	0.30
Chalk	amber	Ref. 1 & 2	10.0	0.17
Cretacious	yellow	Ref. 1 & 2	6.0	0.30
Jurrassic	green	Ref. 1 & 2	16.0	0.20
Zechstein20	blue	Ref. 6	3.7	0.35
Zechstein80	pink	Ref. 6	3.7	0.35
Zechstein	red	Ref. 6	30.0	0.35
Anhydrite	amber	Ref. 1 & 2	50.0	0.35
Ten Boer	yellow	Ref. 1 & 2	18.0	0.18
Upper Slochteren	green	Ref. 8	15.0	0.20
Ameland clay	blue	Ref. 1 & 2	23.0	0.28
Lower Slochteren	pink	Ref. 1 & 2	21.0	0.20
Limburg	red	Ref. 1 & 2	20.0	0.20

Table 1 Elastic material properties for different lithologies

2.2.2 Salt layers

The rock mechanical parameters for the Zechstein and squeezing salt layers are obtained from the thesis of Fokker (Ref. 6). These data have been experimentally validated and compared with the data reported by Liezenberg and Spiers (Ref. 7), and found to be in good agreement.

Since the squeezing salt layer consists of unknown quantities of carnalite and/or Bischofite, it was decided to mimic the rock mechanical properties of this layer by weighted average values of the separate Young's moduli and Poisson's ratios (see Table 2). Since Bischofite is less likely to occur, the majority of the layer is expected to consist of Carnalite, yielding a Young's modulus of 3.7 GPa in Table 1.

	E [GPa]	ν [-]	n [-]	Q/R [K]	A [-]
Halite	30.0	0.35	4.5	8000	2.25E-04
Bischofite	1.8	0.35	3.5	-	2.00E-08
Carnalite	5.5	0.35	5.0	-	4.00E-11

Table 2 Visco-elastic material properties for Zechstein salt

For the elastic models the Young modulus of the squeezing salt layers (Table 1) were assumed to be equal to the average of the stiffness values for Bischofite and Carnalite in Table 2.

The salt-creep in this study is described with the creep model developed by Fokker (Ref. 6) which is available in the program DIANA. In this model even small shear stresses generate creep strains and therefore relax to zero with time, resulting in a hydrostatic stress-situation in the salt.

2.2.3 Producing reservoir

For the producing reservoir (Upper Slochteren) the Poisson's ratio is obtained from laboratory compaction tests using core plugs taken from the Upper Slochteren sandstone formation, i.e. well AME-107 (Ref. 8). These same lab tests also generate values for the compaction coefficient (*Cm*), however, the available samples are of a low porosity and have a limited range only (10-13 %), and therefore they are considered to be not fully representing the Upper Slochteren formation. In order to obtain a relationship of the compaction coefficient as a function of the porosity a mathematical inversion of the leveling measurements is carried out taking into account the porosity (ϕ) distribution of the Upper Slochteren formation. For this the program "SUBSINV" was used, which has been developed by SIEP RTS. The following function was obtained :

$$Cm = 13.9*10^{-5} * \phi - 1.14*10^{-5}$$

with *Cm* in [1/bar] and ϕ in fraction.

The inversion is somewhat uncertain because the leveling could only be done over the (small) part of the subsidence bowl that was on land. Comparing this function with the relations obtained from the limited laboratory tests reveals that the inversion obtained relation lies between the functions of the 1st and 2nd loading experiments (see Table 3). Since it is generally accepted that the 1st loading experiments produce a too high Cm value and that the relationship resulting from the 2nd loading tests may produce a too "flat" *Cm*-ϕ relationship because of the low porosity samples, it is justified to use the relationship from the inversion.

Relation	**Source**
$Cm = 13.9*10^{-5} * \phi - 1.14*10^{-5}$	Inversion of leveling measurements related to porosity map
$Cm = 20.0*10^{-5} * \phi - 1.00*10^{-5}$	Compaction experiments, 1st loading, uniaxial
$Cm = 3.0*10^{-5} * \phi + 0.08*10^{-5}$	Compaction experiments, 2nd loading, uniaxial

Table 3 Compaction coefficient - porosity relationships

The final conversion from compaction coefficient to Young's modulus is then done by

$$E = 3\,K\,(1 - 2\,\nu)$$

and

$$Cm = 1 / (K + 4/3 * G)$$

Alternatively, E values of 11.5 and 15 GPa are used uniformly over the Upper Slochteren formation, this to match the results of previously carried out linear elastic SUBCAL study.

2.3 Depletion scenario

For the years 1990 to 2020, with a time interval of 5 years, the depletion pressures in the Upper Slochteren formation are displayed in Figure 6. These pressure distributions are the result of a reservoir analysis and are performed by NAM. The black frame in these figures is the transition of the finer and coarser grid. The color-scale for all years in Figure 6 is equal. In the blue areas there is no pressure-reduction, while the depletion-pressure is maximum 50 MPa, colored red.

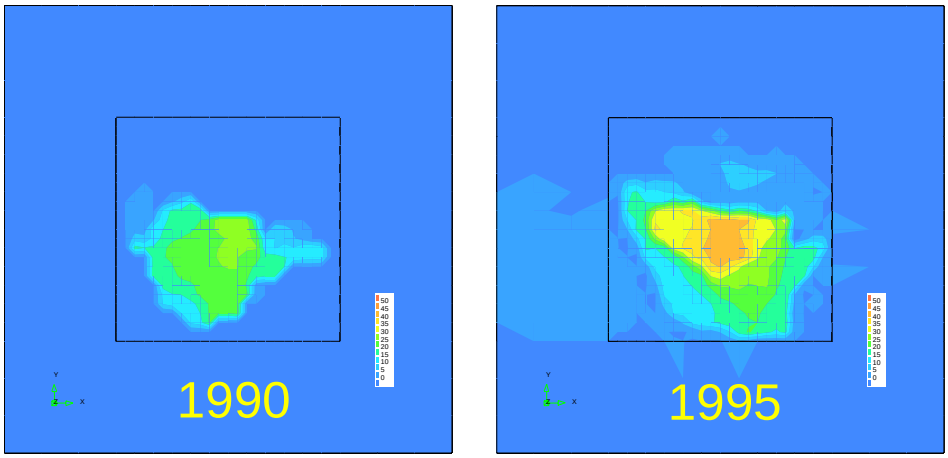

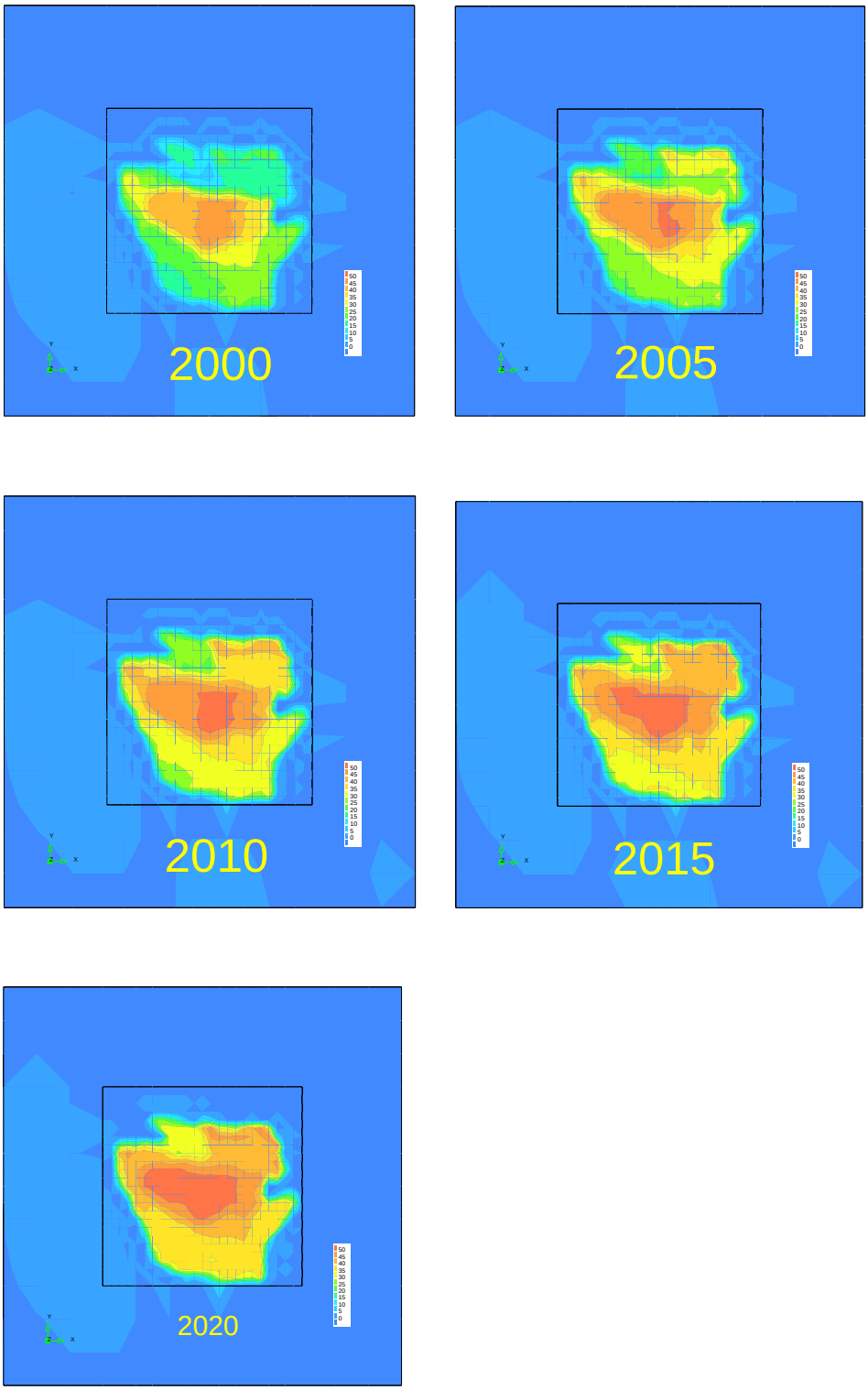

Figure 6 *Depletion pressure distributions in the years 1990, 1995, 2000, 2005, 2010, 2015 and 2020.*

2.4 In-situ stresses

The in-situ stresses gradients are assumed to be constant. The vertical total in-situ stress gradient is assumed to be σ_v = 1 psi/ft = 22.6 kPa/m. The horizontal total in situ stress is assumed to be only depth dependent and not to be affected by the stiffness of the respective layers. The horizontal in situ stress can then be described by:

$$\sigma_h = \sigma_v (1 - \gamma) / \gamma$$

with γ= 0.7. In the Zechstein salt-formation for the horizontal stress is assumed

$$\sigma_h = \sigma_v$$

2.5 Parameter variations

The following parameter variations are performed with respect to the reservoir stiffness where the creep-behavior in the salt is not considered :

- E = 15 GPa
- Stiffness is related to porosity
- E = 11.5 GPa

After these preliminary analyses a serie calculations with the creep-behavior for the Zechstein formation is done. An overview of these analyses is given in Table 4.

Model	**stiffness reservoir**	**20 m layer Zechstein**	**80 m layer Zechstein**	**rest Zechstein**
model1	E = 15 GPa	3.7 GPa	3.7 GPa	30.0 GPa
model2	porosity related	3.7 GPa	3.7 GPa	30.0 GPa
model3	E = 11.5 GPa	3.7 GPa	3.7 GPa	30.0 GPa
model4	E = 11.5 GPa	Halite	Halite	Halite
model5	porosity related	Halite	Halite	Halite
model6	E = 11.5 GPa	Bischofite	Carnalite	Halite
model7	porosity related	Bischofite	Carnalite	Halite
model8	E = 11.5 GPa	Carnalite	Carnalite	Carnalite
model9	porostity related	Carnalite	Carnalite	Carnalite

Table 4 Parameter variation on salt overburden

2.6 Summary of model characteristics

- Linear elastic and visco-elastic (Fokker) material models
- Model-size : 24 x 24 x 5 km

- Element-size : 500x500 m - 2x2 km
- Circa 15.000 brick elements
- Inhomogeneous pressure distribution from reservoir analyses

3. Results

3.1 Preliminary linear elastic analyses

In this section the results of the preliminary linear elastic analyses are presented. There are three models. Two with a constant stiffness of 15.0 and 11.5 GPa, respectively, for the reservoir formation and one with the reservoir stiffness being related to the measured porosity. Figure 7 shows the calculated maximum surface subsidence as function of the depletion pressure profiles for the different time steps. Besides the three curves of the present study the results of a SUBCAL analysis performed by NAM is also shown in this graph. The 15.0 GPa model shows a lower maximum subsidence and the porosity-related model a higher maximum subsidence curve in comparison with SUBCAL results. The 11.5 GPa model is chosen in order to get a good fit of the SUBCAL results.

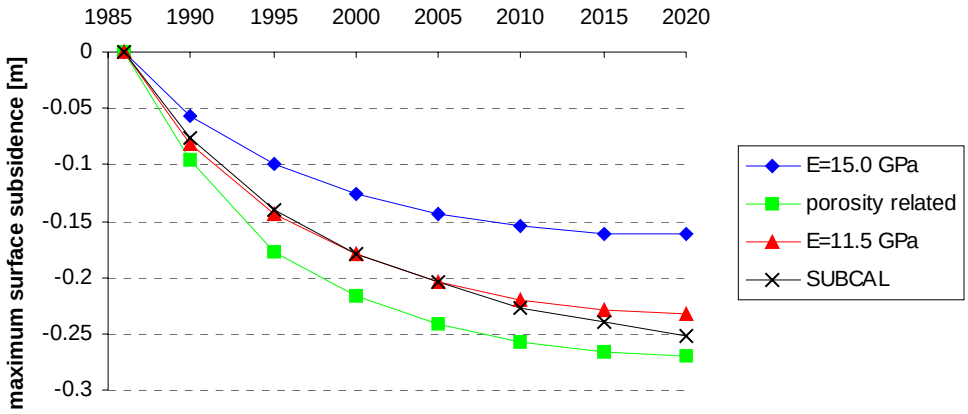

Figure 7 *Maximum subsidence as function of time for a set of models with different reservoir stiffnesses*

The four graphs in Figure 7 look like very similar to each other with a gradual decreasing subsidence velocity and reaching a maximum values in 2015-2020. The maximum calculated subsidence values in 2020 vary from 16 cm for the 15.0 GPa model to 27 cm for the porosity related stiffness model.

In Figure 8, Figure 9 and Figure 10 the surface subsidence in the years 1990 and 2020 is shown for the models with a constant stiffness of E=15.0 GPa, a porosity related stiffness and a constant stiffness of E=11.5 GPa, is shown, respectively. The color-scale in all these figures is equal. The calculated surface subsidence bowl tends very gradually to one centrally located maximum. For these three models the location of the maximum subsidence travels in North/Eastern direction with time.

The subsidence bowl in 2020 is not only deeper but also wider than in 1990. From the figures it can be seen that the subsidence bowl of the porosity related stiffness model is differently shaped. For this model the subsidence above the lower porosity North edge of the reservoir is clearly less so that the bowl is more oval shaped than the other models. The subsidence gradients are very low in all cases.

In Figure 11, Figure 12 and Figure 13 the compaction strain distribution in the years 1990 and 2020 is shown for the models with a constant stiffness of E=15.0 GPa, a porosity related stiffness and a constant stiffness of E=11.5 GPa, respectively. In these figures the color-scale varies form red (dilatancy of 0.02 %) to blue (compaction of 0.3 %). As the surface subsidence shows a very gradual path to a central located point with the maximum value, the distributions of the compaction strains show strong changes in distribution. From these figures the depletion area can be clearly recognized by strongly changing colors (compaction values) at the edges of the reservoir. As the surface subsidence bowls have a very smooth shape, the shape of the compacted areas in the Upper Slochteren formation is very capricious. The compaction strain distribution for both models with a constant Upper Slochteren stiffness show agreement with the depletion pressure distributions of the same years in Figure 6. In 1990 a small area in the South/Western corner is depleted and the pressures are almost constant in the depleting area, while in 2020 the depleting area is considerably larger with stronger pressure changes in a central East-West band in the reservoir with a branch in North/Eastern direction. These characteristics can be recognized in the compaction strain distribution in the Upper Slochteren formation for both models with a constant stiffness in this layer. However, the model with the porosity related stiffness of the Upper Slochteren formation shows a different compaction pattern. In the 1990 compaction strain distribution a blue area is recognized, pointing to a weak spot (high porosity) in the formation. The 2020 distributions show for the porosity-related stiffness model a clearly lower compaction level at the North edge of the reservoir than the constant stiffness model. This agrees to the measured lower porosity in this area and the related higher reservoir stiffness.

In Figure 14 to Figure 22 the total horizontal and vertical stress distribution in 1990 and 2020 are shown for all three models, respectively. For all three models the total horizontal stress changes in the East/West direction (Sxx) are circa 10 % larger than the total horizontal stress changes in the North/South direction (Syy), while the total vertical stresses changes are less than 10 % of the total horizontal stress changes. As the reservoir is depleted the stresses in and around the reservoir are re-distributed yielding a stress reduction in the reservoir itself and stress increase in the area just around the reservoir.
For the porosity related model in 1990 the maximum depletion pressure is 27.2 MPa while in this area the total horizontal stress is circa 20 MPa and the total vertical stress is circa 5 MPa, yielding $\gamma_H = 20/27.2=0.74$ and $\gamma_Z = 5/27.2 = 0.19$. For the porosity related model in 2020 the maximum depletion pressure is 52.4 MPa while in this area the total horizontal stress is circa 40 MPa and the total vertical stress is circa 10MPa, yielding $\gamma_H = 40/52.4 =0.76$ and $\gamma_Z = 10/52.4 = 0.19$.

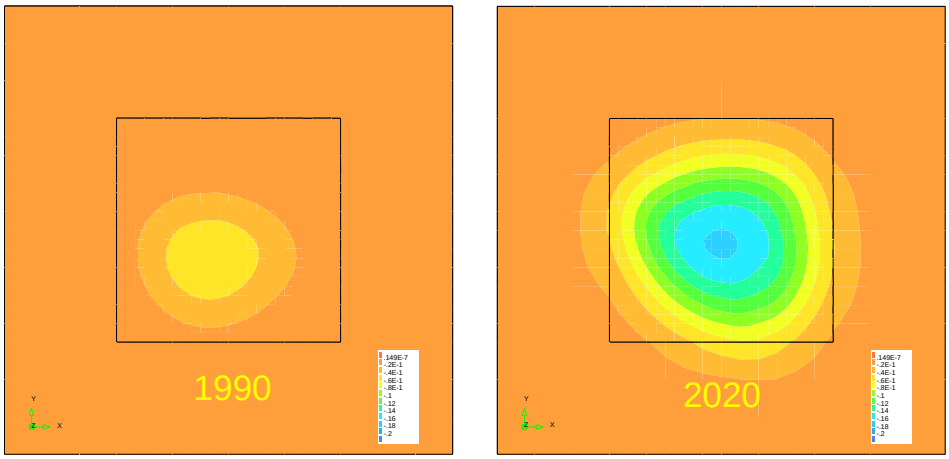

Figure 8 Seabed subsidence for the E = 15.0 GPa model in the years 1990 and 2020

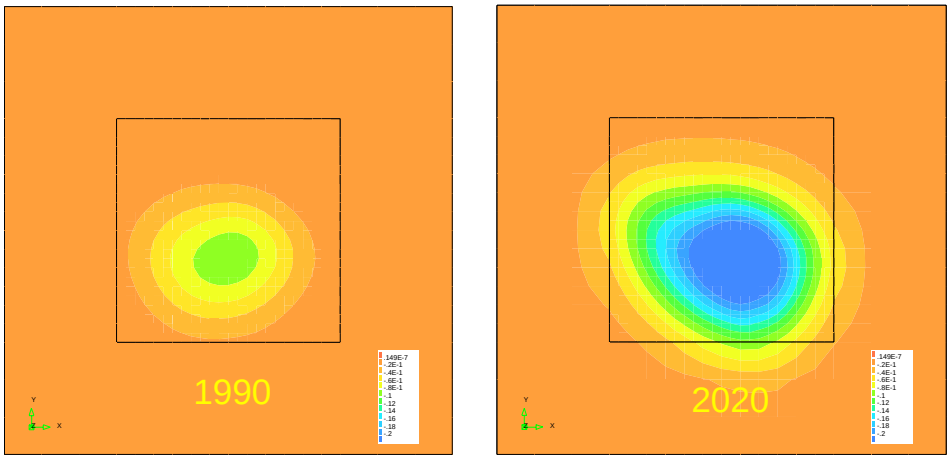

Figure 9 Seabed subsidence for the porosity related stiffness model in these years

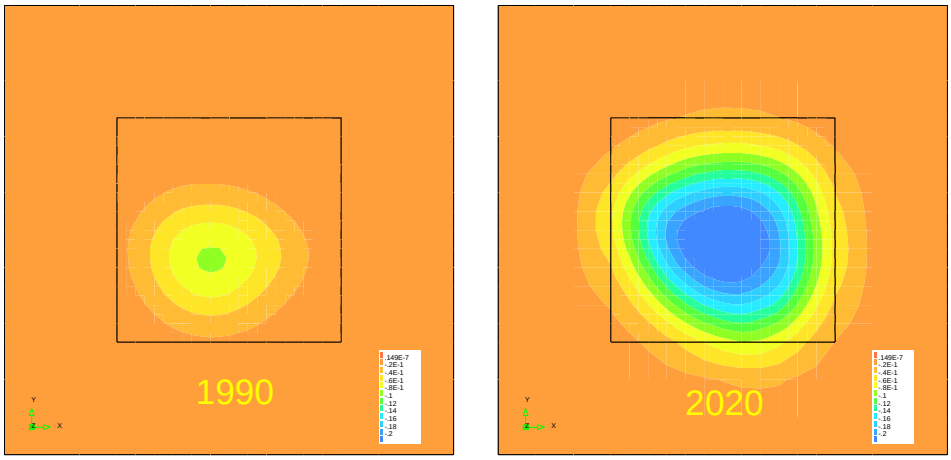

Figure 10 Seabed subsidence distribution for the 11.5 GPa model in these years

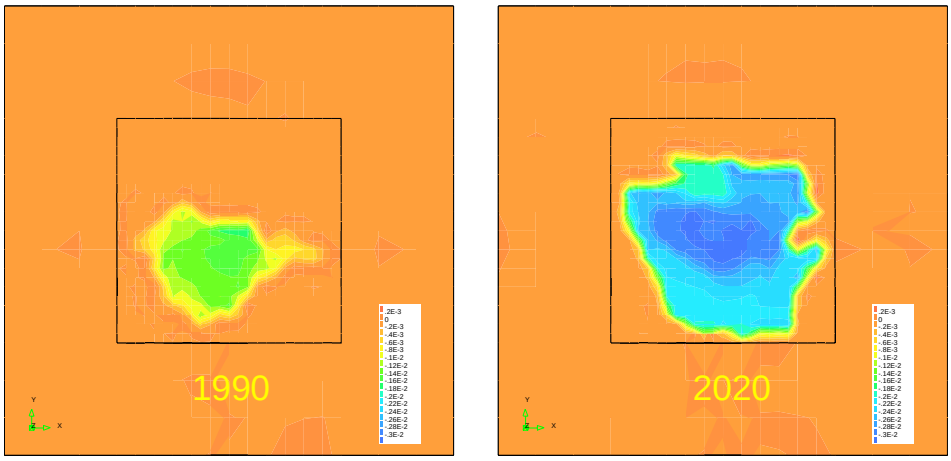

Figure 11 Reservoir compaction for the E = 15.0 GPa model

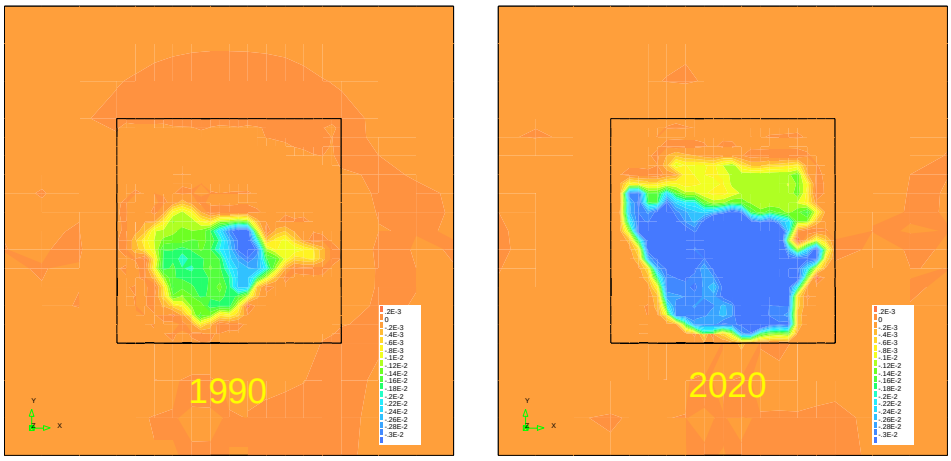

Figure 12 Reservoir compaction for the porosity related stiffness

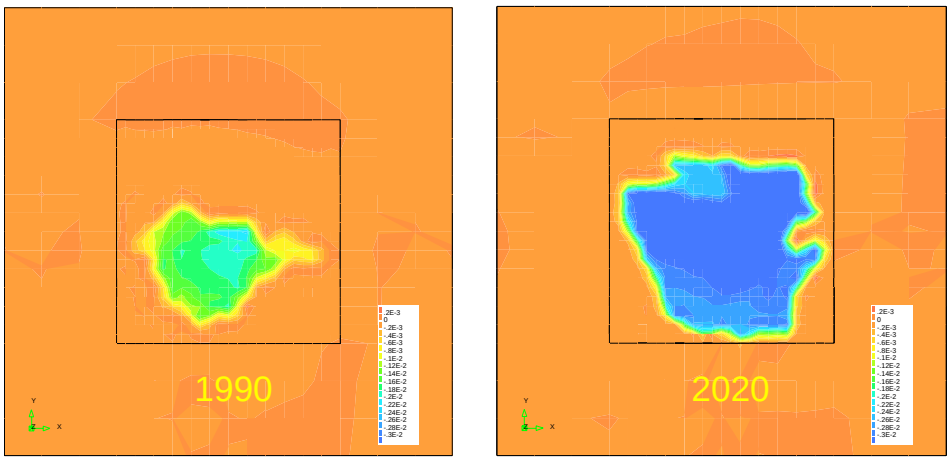

Figure 13 Reservoir compaction for the 11.5 GPa model

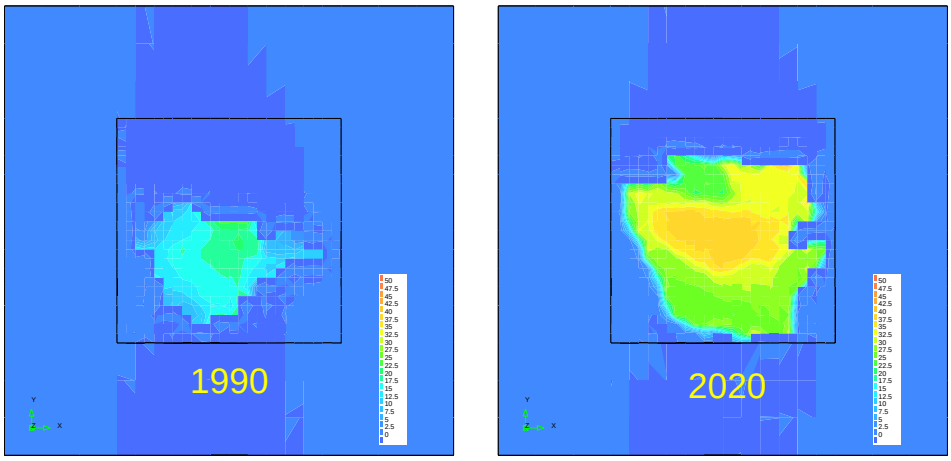

Figure 14 Horizontal total stress (Sxx) changes for the E = 15.0 GPa model

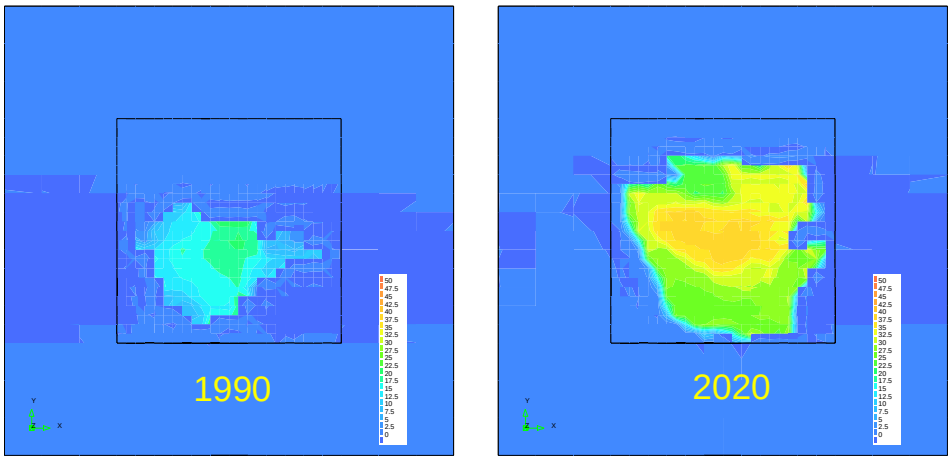

Figure 15 Horizontal total stress (Syy) changes for the E = 15.0 GPa model

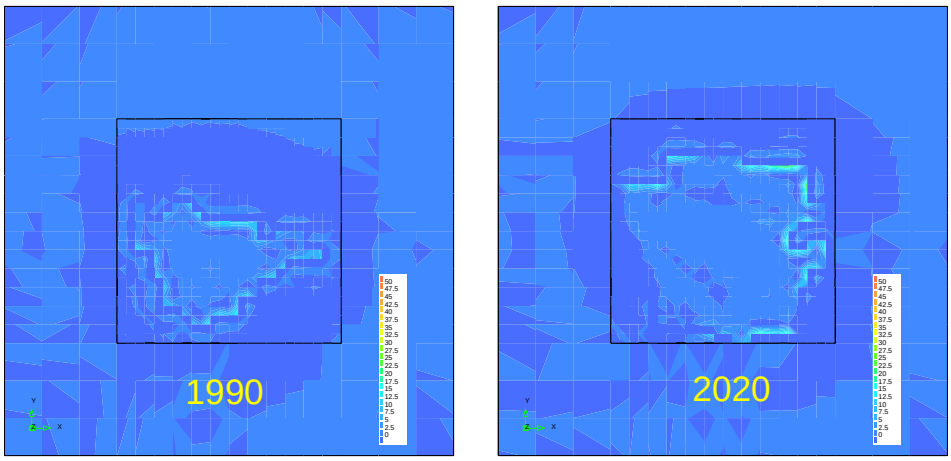

Figure 16 Vertical stress changes for the E = 15.0 GPa model

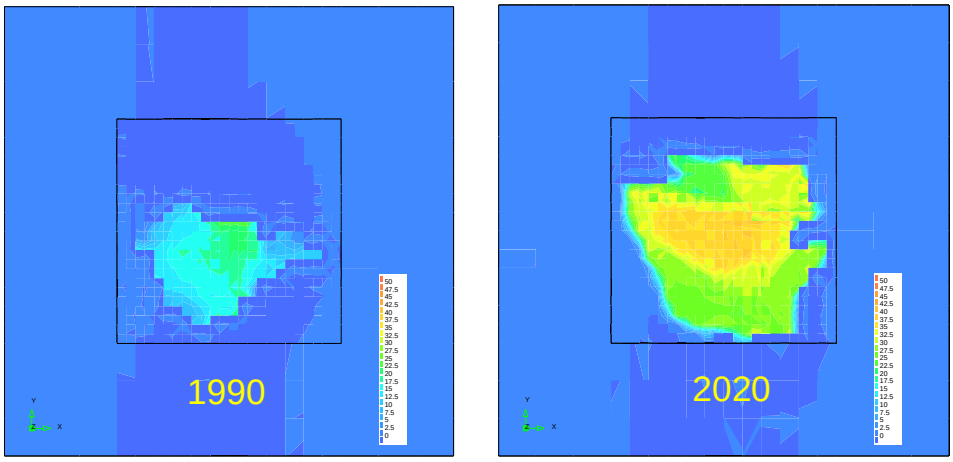

Figure 17 Horizontal total stress (Sxx) changes for the porosity rel. stiffness model

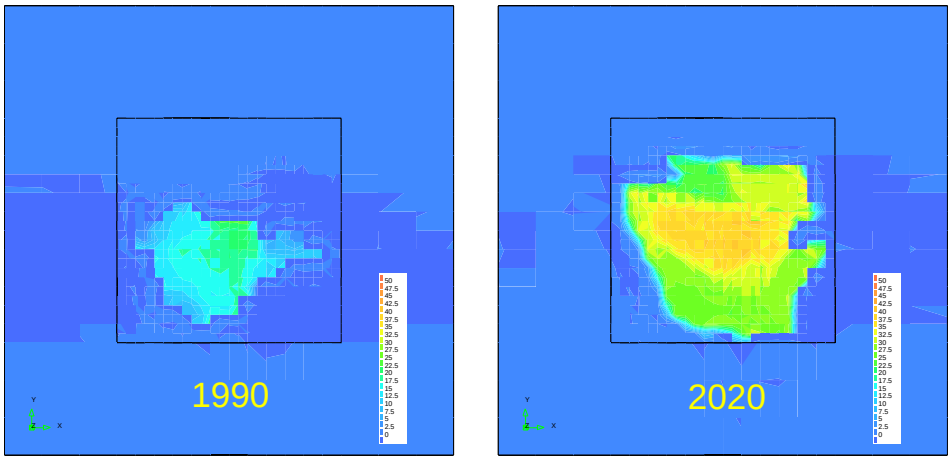

Figure 18 Horizontal total stress (Syy)changes for the porosity rel. stiffness model

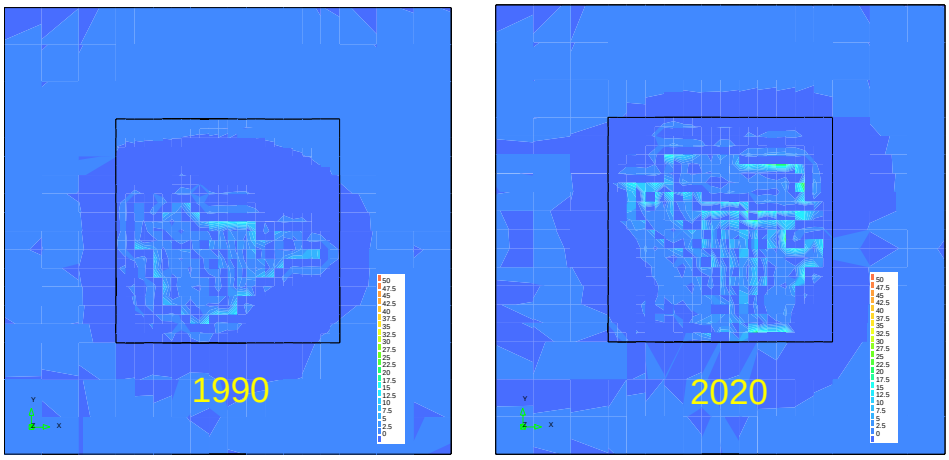

Figure 19 Vertical total stress changes for the porosity rel. stiffness model

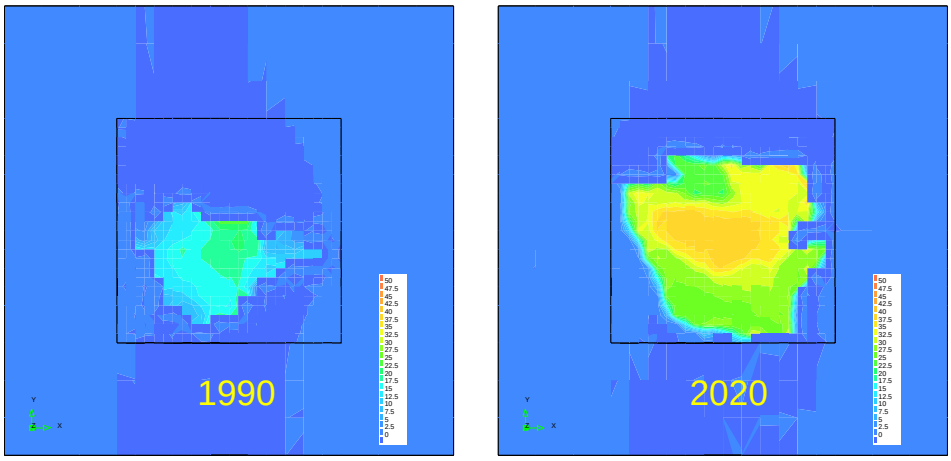

Figure 20 Horizontal total stress (Sxx) changes for the E=11.5 GPa model

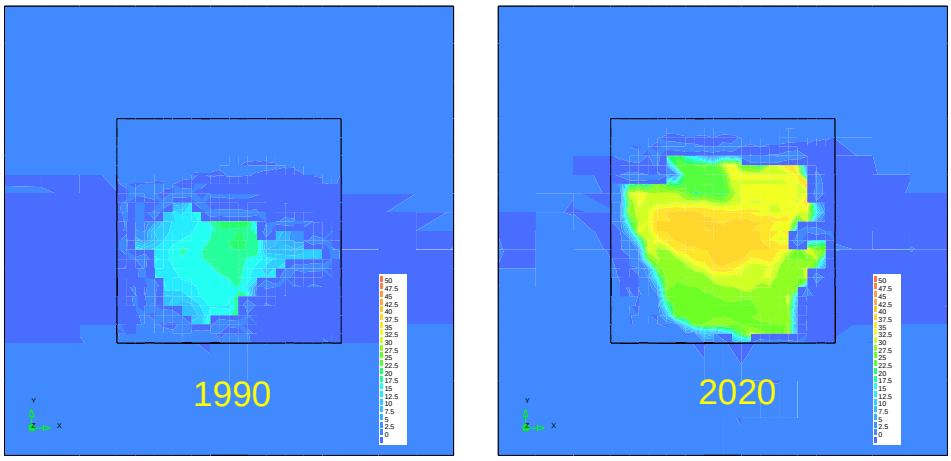

Figure 21 Horizontal total stress (Syy) changes for the E=11.5 GPa model

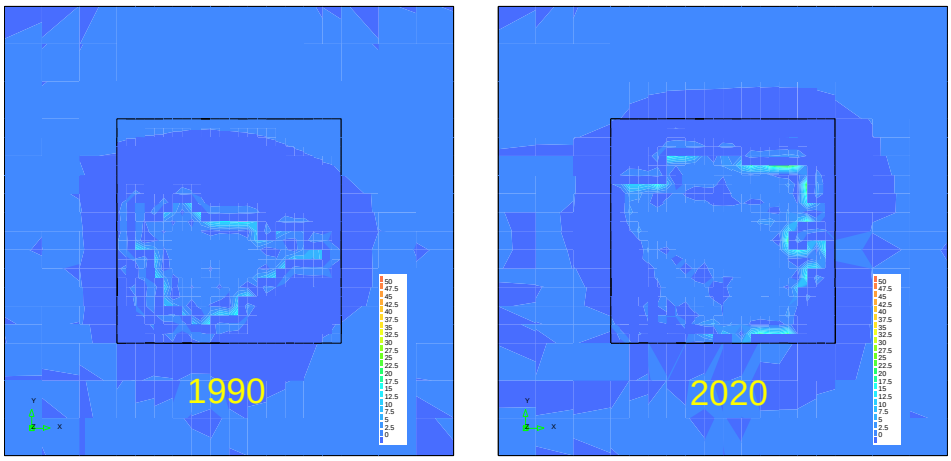

Figure 22 Vertical total stress changes for the E=11.5 GPa model

3.2 Result of salt-creep models

3.2.1 Salt-creep models with porosity related reservoir stiffness

In this section the results of the salt-creep models defined in section 2.5 are described and discussed. As the 15.0 GPa models are considered too stiff, they are not analyzed in combination with the salt-creep. In Figure 23 the maximum subsidence as function of time is shown for the porosity related stiffness models with salt-creep behavior. In this figure the model2 from Table 4 is indicated as elastic 11.5 GPa Halite model, model5 as the porosity related Halite model, model7 as the porosity related Bischofite/Carnalite/Halite model and model9 as the Carnalite model. Further, in Figure 23, results of the NAM SUBCAL calculations and the measured maximum surface-subsidence until 1998 are shown.

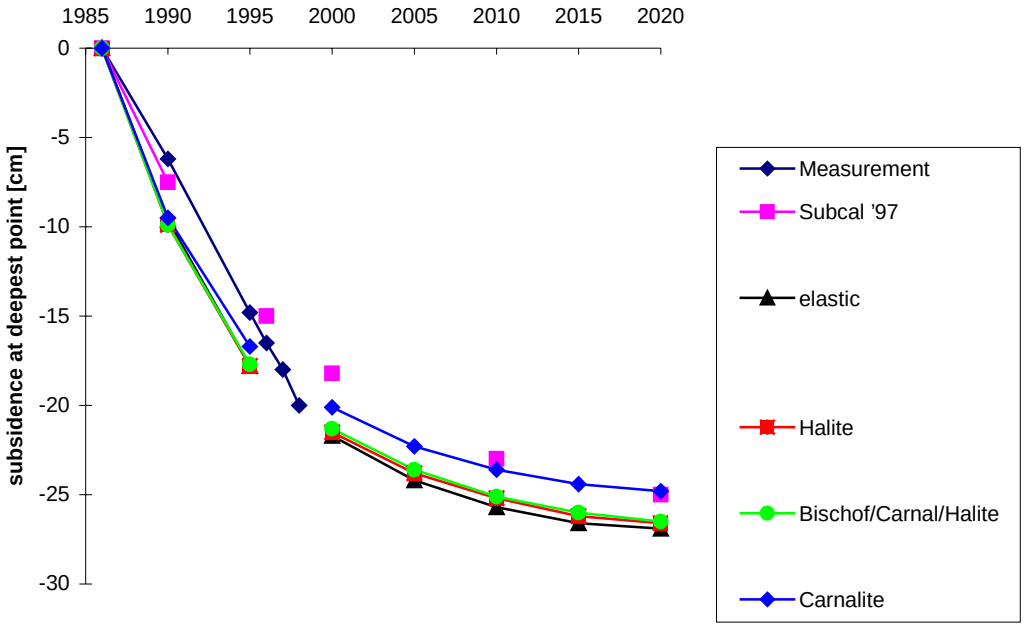

Figure 23 *Creep effects of Zechtstein on maximum subsidence for the model with porosity related stiffness*

In Figure 23 the maximum subsidence as calculated for the different creep models as well as the measured maximum subsidence and the calculated SUBCAL results are shown as function of time. In order to make the measured subsidence results clearly visible the connecting lines in the creep-model graphs between 1995 and 2000 are omitted. It can be concluded that predicted subsidence from the numerical creep model is initially a little too high, but that the calculated subsidence speed reduces from 1995 onwards, while the observed subsidence speed remains constant.

From Figure 23 it can be concluded that the different salt-models yield only small differences with respect to the maximum subsidence. Apparently, the shearstresses in the salt formation are so small that the related creep effects can be neglected. In Figure 24 the equivalent shear stress distribution in the squeezing Zechstein layer are displayed for the years 1990 and 2020. Note that the maximum value on the color-scale in this figure is not higher than 2.5 MPa, while in all the other stress plots until now the maximum value is 50.0, which is a factor 20 higher. From this figure it can be concluded that the shear stresses in the squeezing layer are indeed very low. Only in the squeezing layer just above the South/Western corner some shear stresses can be noticed, and in all other corners the shearstresses are almost zero in the squeezing Zechstein layer.

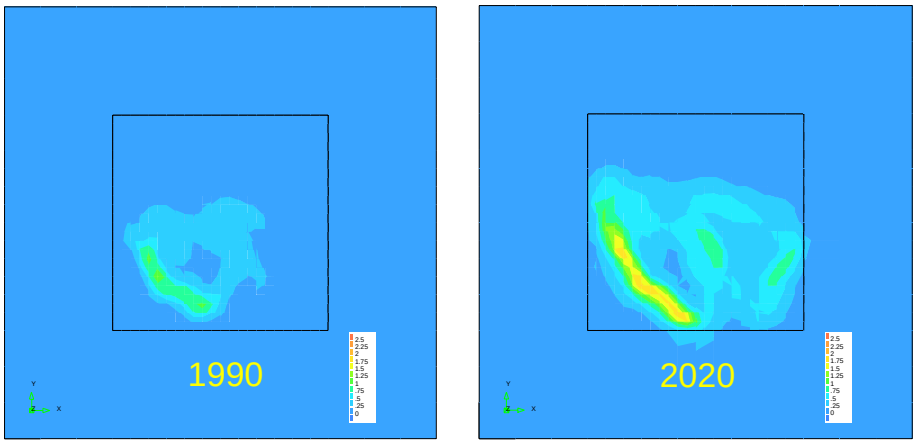

Figure 24 *Equivalent shearstress in squeeze layer for model with porosity related stiffness in the years 1990 and 2020*

The Figure 25 shows a cross-section through the model from South/West to North-East. The squeezing layer is identified with blue (5th from top) and at the left side of this figure the Zechstein formation appears to be so thin that squeezing layer, which is at the top of the Zechstein formation, approaches the reservoir (green, 10th from top) very closely. The Figure 26 and Figure 27 depict the equivalent shear stresses in this cross-section in the years 1990 and 2020, respectively. These figures show that outside the reservoir itself the shear stresses are concentrated to the edges of the reservoir.

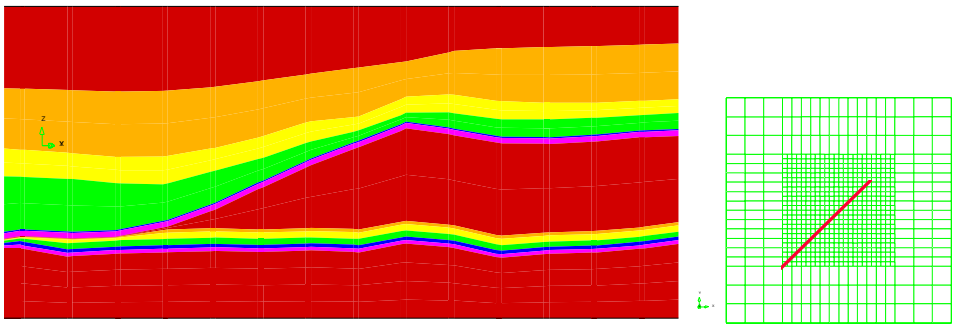

Figure 25 Formation layers in cross-section

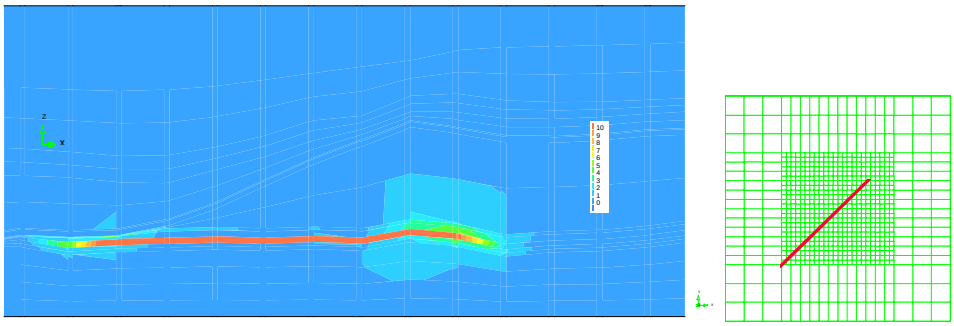

Figure 26 Von Mises stresses in cross-section in the year 1990

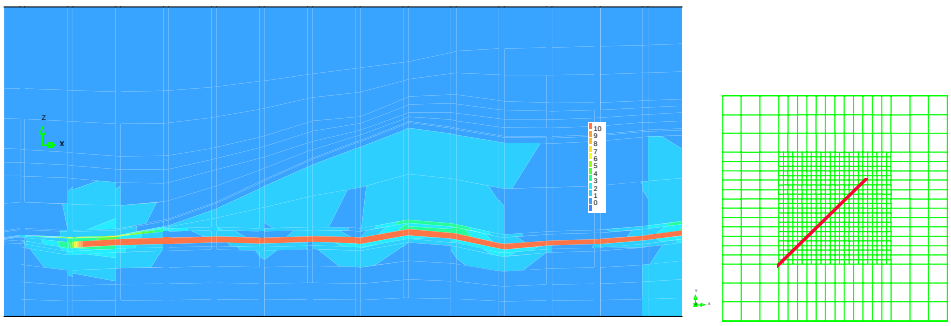

Figure 27 Von Mises stresses in cross-section in the year 2020

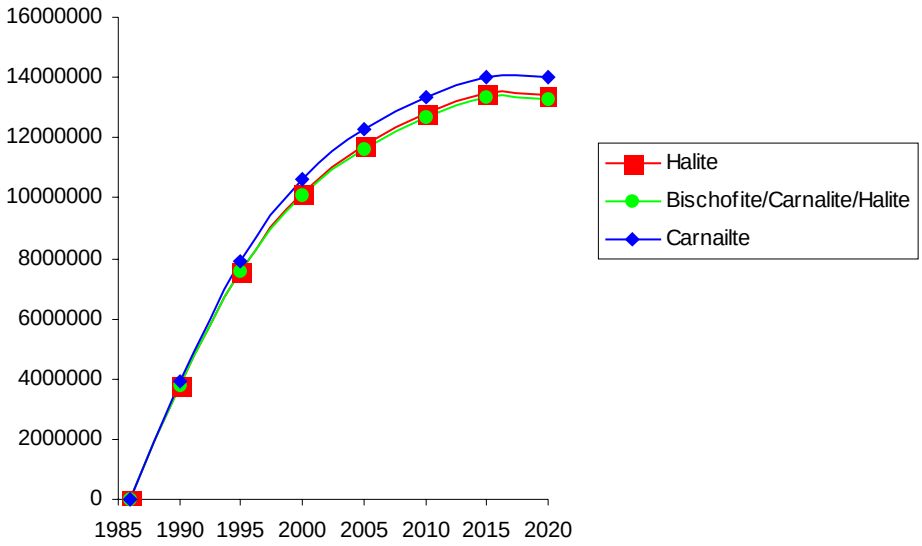

Figure 28 *Volume [m3] of surface subsidence bowl as function of time for the model with porosity related stiffness*

The volume of the surface subsidence bowl as function of time for the different creep models with the porosity related reservoir stiffness is depicted in Figure 28. The volume increases gradually to a constant value of 14 million cubic meters. In the last two time-steps (since 2010) the volume does not changes very much any more.

3.2.2 Salt-creep models with 11.5 GPa reservoir stiffness

In this section the results of the creep models with a constant reservoir stiffness of 11.5 GPa are presented and discussed. The stiffness of 11.5 GPa was chosen in order to match the maximum subsidence at surface as good as possible to the subsidence resulting from SUBCAL. In fact this assumption yields to an underestimation of the measured surface subsidence.

Figure 29 displays the creep-effects of model6 (E=11.5 GPa for reservoir and Halite for salt), model8 (E=11.5 GPa for reservoir and Bischofite/Carnalite/Halite for salt) and model10 (E=11.5 GPa for reservoir and Carnalite for salt). Also the elastic model results, the SUBCAL results and the measured maximum subsidence are shown in this figure. From this figure it can also be concluded that the results for the different creep models do not differ very much. The calculated and measured maximum subsidence trajectory in the interval 1986-1995 agree very well, however, since 1995 the calculated subsidence speed reduces strongly, while the measured subsidence remains more or less constant.

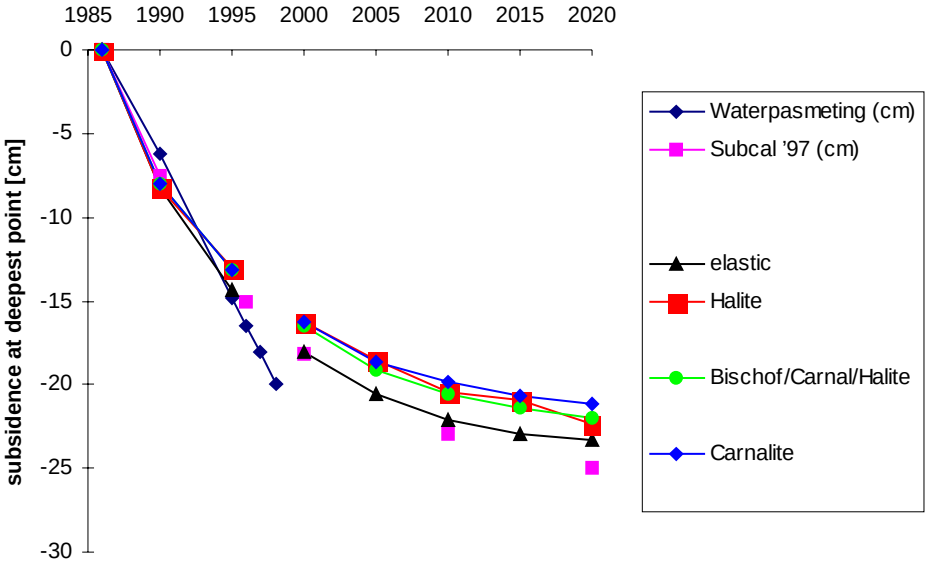

Figure 29 Creep effects of Zechstein on maximum subsidence for the E=11.5 GPa model

Figure 30 to Figure 33 are equivalent to the Figure 24 to Figure 27 and show that for the model with a constant reservoir stiffness the shear stresses in the squeeze layer are not high enough in order to cause significant creep in the salt-layers.

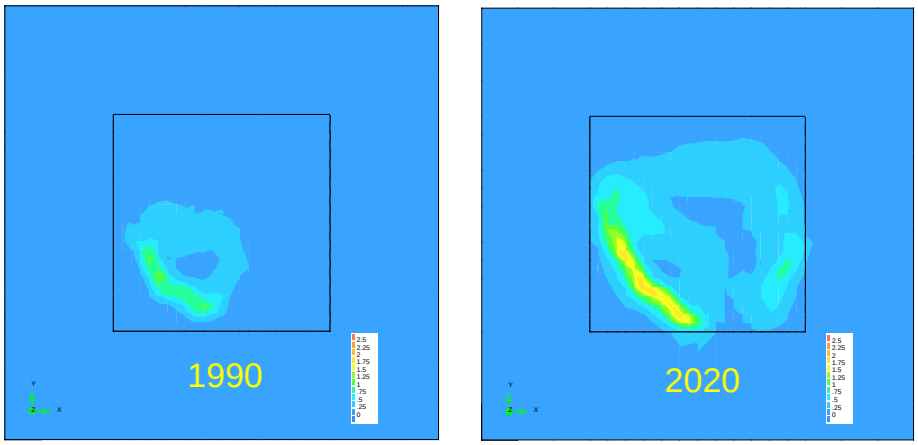

Figure 30 Von Mises stress in squeeze layer for 11.5 GPa model in the years 1990 and 2020

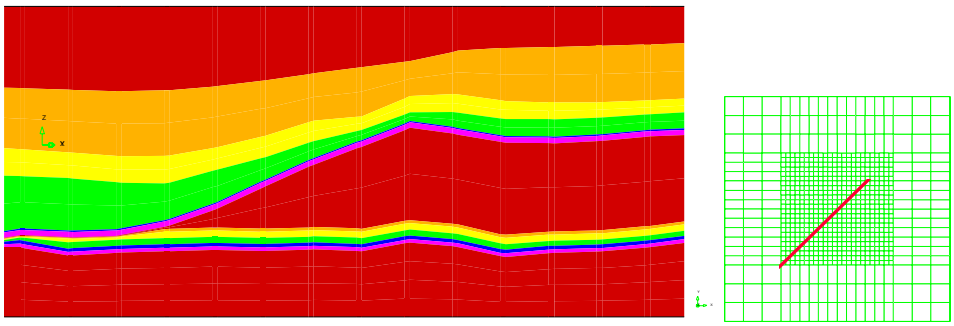

Figure 31 Formation layers in cross-section

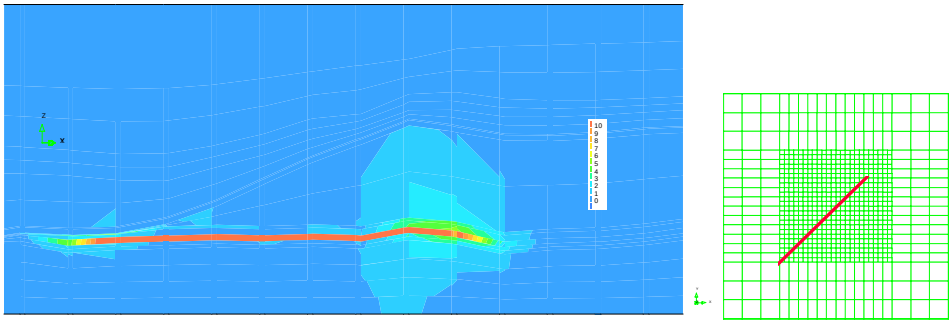

Figure 32 Von Mises stresses in cross-section in the year 1990

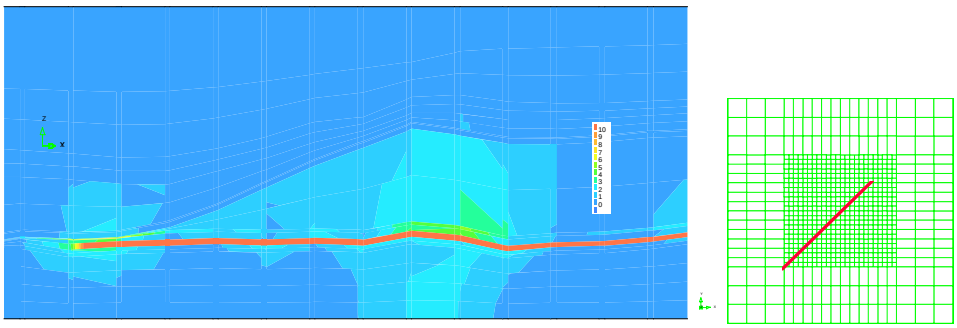

Figure 33 Von Mises stresses in cross-section in the year 2020

The volume of the surface subsidence bowl for the creep model with the 11.5 GPa reservoir stiffness is given in Figure 34. As the maximum bowl volume is for the porosity-related stiffness models between 13.5-14 million cubic meters at the end of field life, this is between 15-16.5 million cubic meters for the models with a constant reservoir stiffness of 11.5 GPa. As the maximum surface subsidence values of the latter model are considerably lower, the width of the subsidence bowls of the constant reservoir stiffness models must be clearly larger than the width of the porosity related stiffness model. This agrees to the conclusion with respect to the preliminary elastic models that the subsidence bowl for the porosity related stiffness model at the North edge of the reservoir is shallower.

Based on the above observations, it can be concluded that the calculated increased subsidence, compared to SUBCAL in 2020, is a result of the specific (lower) stiffness of the individual layers in the overburden, rather than by creep of salt. This becomes apparent when the results of the salt model calculations are compared with the elastic ones and the results from the SUBCAL simulations.
The porosity related stiffness case shows large compactions and top-reservoir subsidence in a small North/South elongated subsection of the reservoir, which can be seen best in the worst case model (constant pressure) of Figure 37. This is not seen in the constant (11.5 GPa) stiffness case, which shows a more 1-dimensional behavior.
As a result there may be more arching above this high porous reservoir subsection and hence more unloading in the thick overlying salt-layer. It can indeed be seen that the case with the lowest salt stiffness (full Carnalite case) shows least subsidence as a result of this unloading. The pure Halite case and the Halite with 80m/20m Carnalite/Bischofite show little difference since the average stiffness of the salt is virtually the same. Also the more 1-dimensional constant (11.5 GPa) stiffness case is not very sensitive to the stiffness of the salt overburden layers in general.

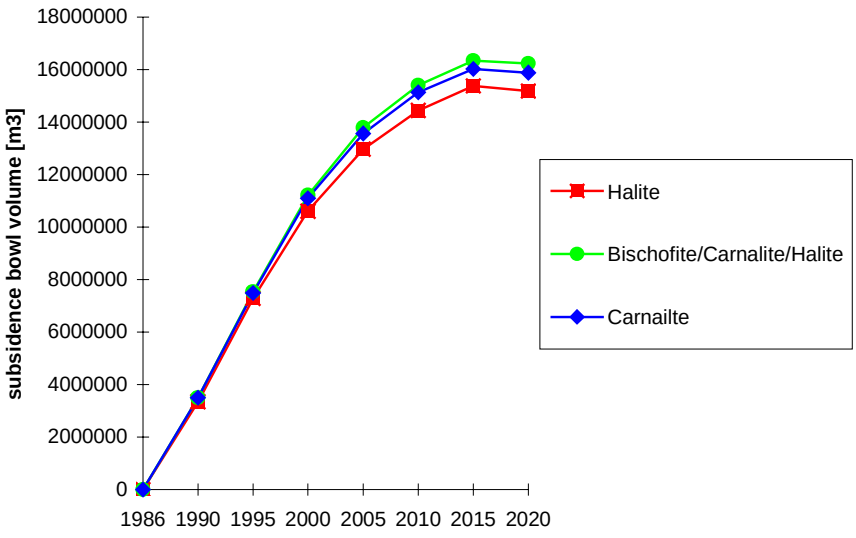

Figure 34 *Volume [m3] of surface subsidence bowl as function of time for the model with constant E=11.5 GPa stiffness*

3.3 Results of the worst case model

From the previous analyses it was concluded that creep is not significantly affecting the surface subsidence. Comparing the measured surface subsidence and the previously presented analysis results, some concerns remain on the surface subsidence

speed. While all the analyses tend to a slowing down of the subsidence speed in the period 1995-2000, the leveling measurements show a constant speed. A factor that may have large effect on the results, but is not considered until now is the depletion pressure distribution resulting from the reservoir analysis. Therefore, one more model is defined, that should be considered as a worst case model with respect to the depletion pressure distribution. This worst case model is characterized by the following assumptions:

- No creep
- Stiffness in reservoir is porosity related
- Depletion pressure is assumed to be constant at the maximum depletion pressure over the full reservoir. That means that the depletion pressure profiles in Figure 6 are modified in such a way that for all the locations were the depletion pressure is nonzero, it is set to 1.

As the worst case model is a linear elastic model, the maximum surface subsidence is proportional to the depletion pressure for the chosen reservoir definition.

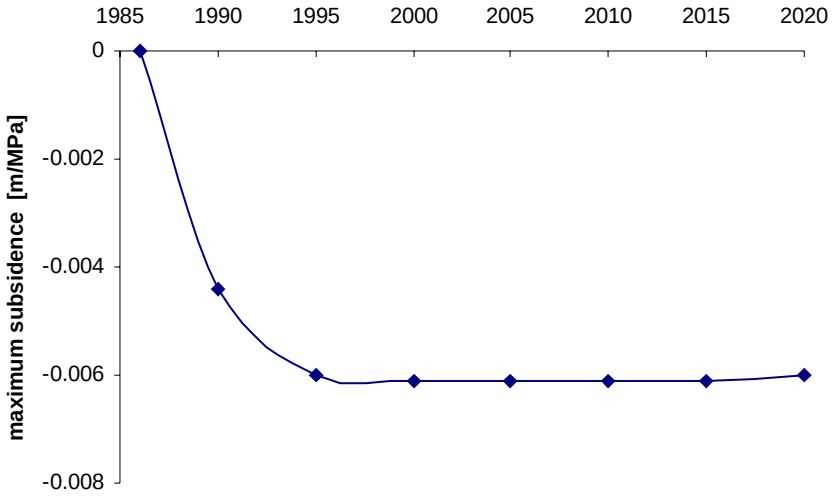

Figure 35 Maximum surface subsidence [m/MPa] for a unit depletion of the worst case model.

The maximum surface subsidence for a unit depletion of the worst case model is depicted in Figuur 35.. This figure shows that the maximum subsidence for unit depletion is already reached in 1995. From the depletion pressure distribution pictures in Figure 6 it can be concluded that the depleting area does not change any more after 2005 and that in the period 1995-2005 only the Northern edge of the reservoirs changes, while the other edges remain constant. Apparently, the stiffness in the North part of the reservoir so high that depletion of this area hardly affects the subsidence at surface.

In Table 5 the maximum depletion pressure for the pressure profiles in section 2.3 are listed. These pressures result from a reservoir analysis performed by NAM. In this depletion pressure scenario the gas-pressure reduces maximum 52 MPa, which level is reached in 2005.
Multiplication of the maximum surface subsidence for unit pressure in Figuur 35, with the depletion pressures in Table 5 yield the total surface subsidence for the worst case model, depicted in Figure 36. The surface subsidence of the worst case model grows very fast to a level of circa 26 cm in 1995 and than slows down strongly coming to a maximum value from circa 32 cm. For the defined reservoir size and the maximum depletion pressure of 52 MPa the surface subsidence of 32 cm must be considered at the maximum.

Year	1985	1990	1995	2000	2005	2010	2015	2020
Pressure [MPa]	0	27.2	43.2	49.1	51.7	52.2	52.5	52.4

Table 5 Maximum depletion pressure for the pressure profiles in section 2.3

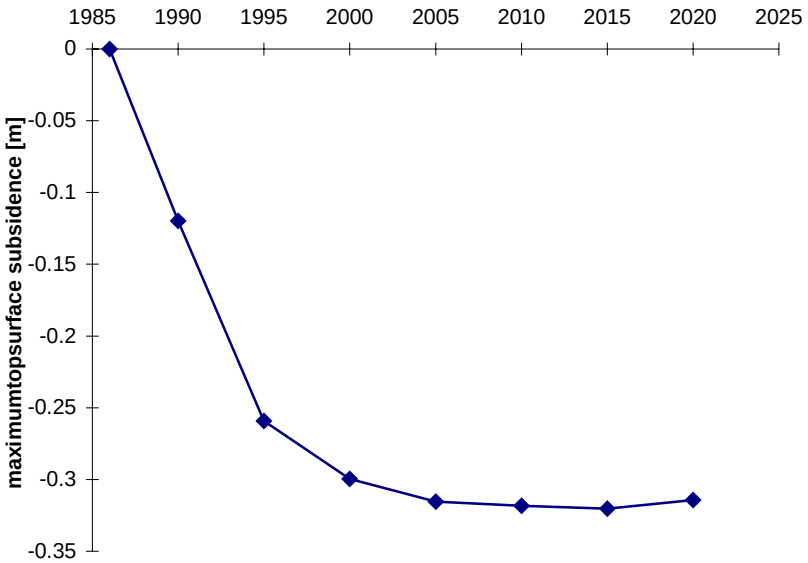

F *del with the*

T in Figure
3 r subsi-
d ıe porosity
r

F ervoir
d e non-
c ous reser-
v tively) are

almost equal, which agrees to what has been noticed at surface level. These figures also show a smooth gradient of the top-reservoir subsidence at the North edge of the reservoir, which is the result of the stiffer formation at this location.
The surface subsidence for the worst case model under unit depletion is depicted in Figure 38 for the years 1990, 2000 and 2020.

In Figure 39 the reservoir compaction distribution for the worst case model is shown.

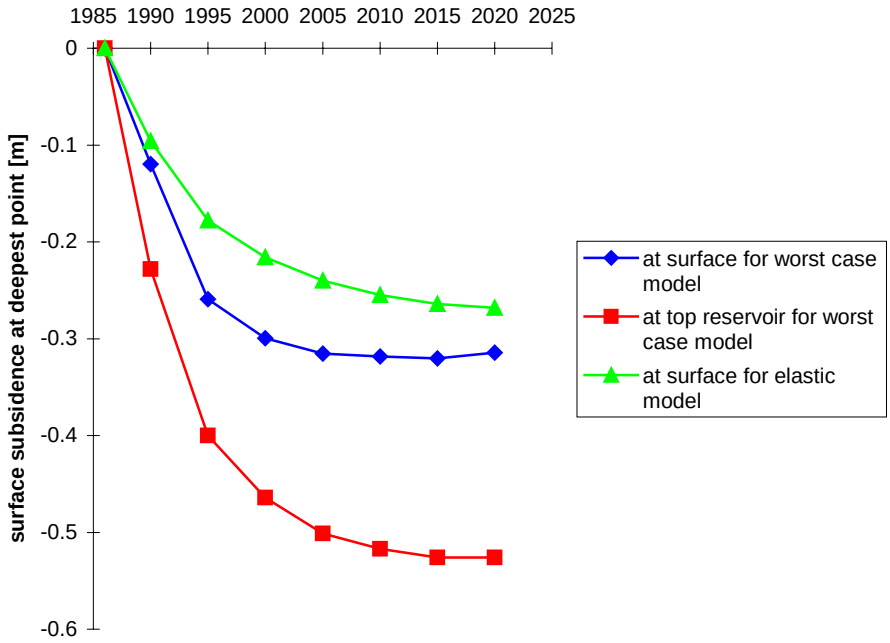

Figure 37 Maximum surface subsidence in worst case model

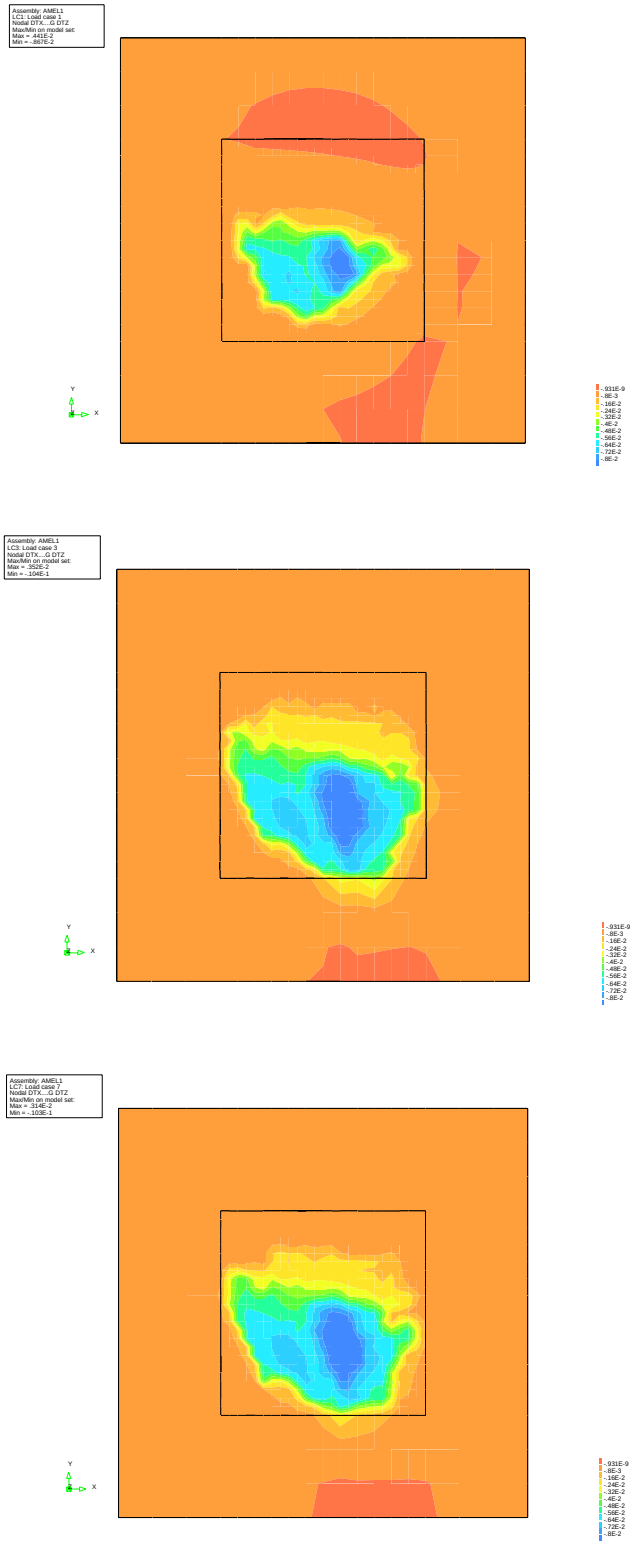

Figure 37 *Worst case model top-reservoir subsidence results in the years 1990, 2000 and 2020 with unit depletion pressure*

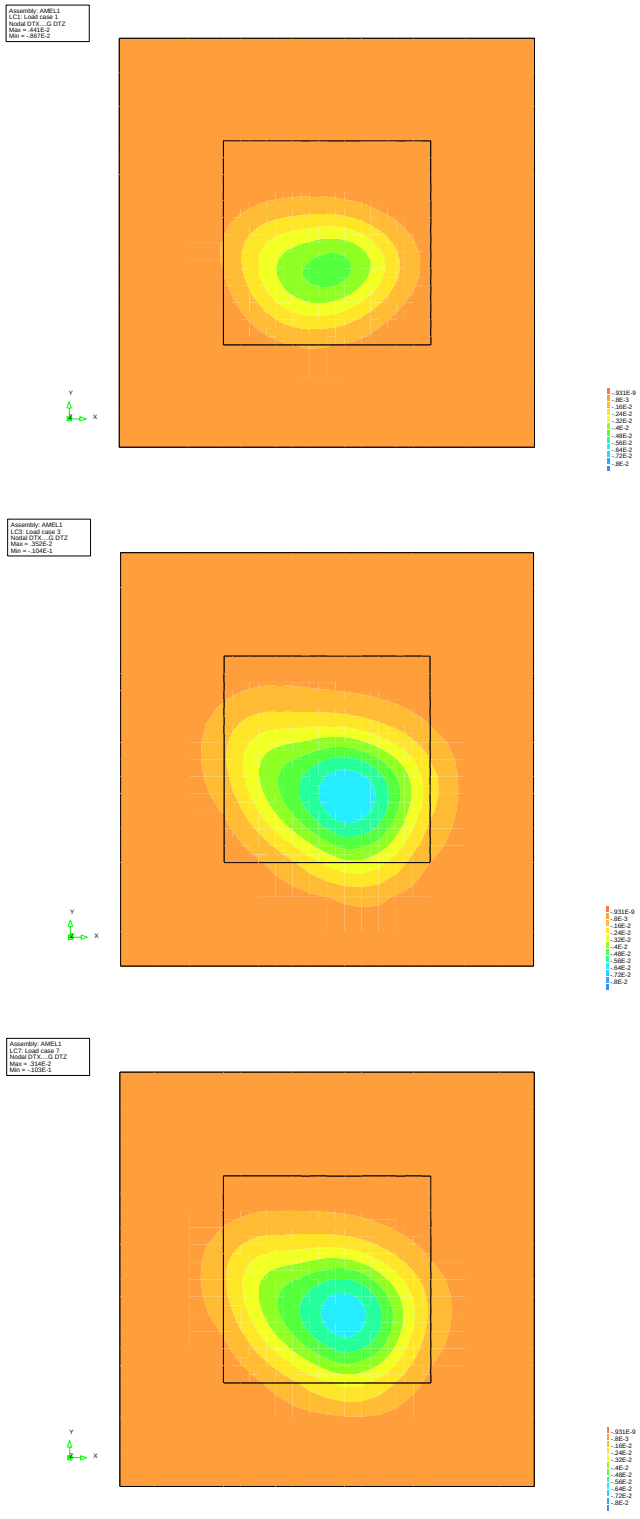

Figure 38 *Worst case model seabed subsidence results in the years 1990, 2000 and 2020 with unit depletion pressure*

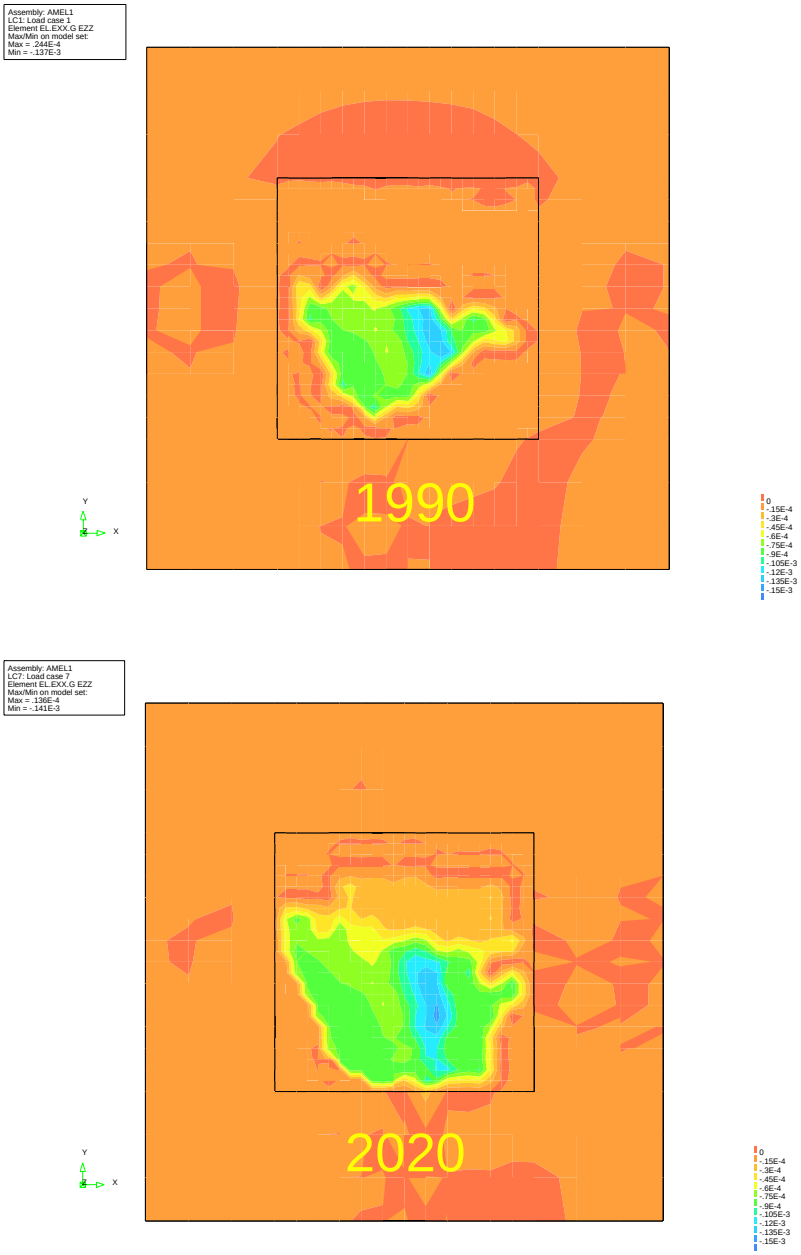

Figure 39 *Worst case model compaction strain results in Slochteren with unit depletion pressure in the years 1990 and 2020*

4. Conclusions

From this study it is concluded that:

- The model with porosity related stiffness for the reservoir is characterized by a weak (high porous) spot in the center of the reservoir and a very stiff (low porosity) ridge at the Northern edge of the reservoir. The shape of the surface subsidence bowl of the model with porosity related stiffness is more oval in East-West direction, while the subsidence bowl for the model with constant reservoir stiffness is more circular. In general the surface subsidence bowl of the porosity related reservoir is deeper with a smaller width than the models with a constant reservoir thickness.
- The calculated maximum surface subsidence with the porosity related stiffness model matches very well with the measured subsidence in the year 1998. From then on the analysis results show a strong slowing down of the subsidence, while the measured subsidence rather shows a constant speed.
- The shear-stress resulting from initial compaction is not sufficiently high in order to cause significant creep in the squeezing Zechstein layers. Therefore it is concluded that salt creep-effect of the Zechstein formation can not explain the differences between the elastic models and the measured subsidence. This is also supported by the finding that the subsidence is not larger in case of thicker squeezing salt layers.
- As the depletion pressure distribution, together with the reservoir dimensions, are important factors in the model, a worst case model has been defined with the assumption that the gas-pressure reduction is constant at the maximum level over the total reservoir. In this model a porosity related stiffness for the reservoir is assumed. This model shows a very strong increase of the subsidence in the period 1985-2000, when the depletion pressure increases from zero to circa 52 MPa. A very strong slowing down of the subsidence in the year 2000 when the maximum depletion level has been reached. From this model it is concluded that the maximum surface subsidence is found to be circa 32 cm, while the maximum surface subsidence in the year 2000 is circa 30 cm.
- A realistic estimate for the maximum surface subsidence at the end of reservoir life is 26.5 cm and the worst case estimate is 32 cm. The maximum value for compaction strain is 0.3 % in the major part of the reservoir with a considerably lower value of 0.15 % in the Northern part of the reservoir. The maximum volume of the surface subsidence bowl is estimate at 14 million cubic meters at end of field life.

5. References

1. Peterson, T. (XGP/3) “Ameland Vp & densities”, internal NAM e-mail communication 26-05-98
2. Dankbaar, J.W.M. (XGP/23) “S-Well data”, internal NAM e-mail communication 08-06-98
3. Veeken, C.A.M. “Rock Mechanics Manual Part 1 - Introduction and Basics”, RKMR.93.052 (EP94-1993). pag. 142, January 1994
4. Roest, J.P.A. et. Al. “Geomechanical modeling of the Roswinkel gas field”, TU-Delft report TA/IG/98/15, June 1998
5. Schreppers, G. “Compaction study of the Groningen gas field”, Draft TNO-report 98-MIT-NM-R/0467, April 1998
6. Fokker, P.A. “Behavior of Salt and Salt Caverns”, Ph.D. Thesis TU-Delft, January24th 1995.
7. Liezenberg, J.L., Spiers, C.J. and Peach, C.J. “A thermo-mechanical data base for rock types expected in and around Permian evaporate bodies in the Netherlands”, Institute of Earth Sciences, University of Utrecht, January 1995.
8. Compaction experiments on AME-107 & M09-3 cor plugs, SIEP-RTS, in preparation.